ISSN: 0067-2904

Evaluation of Laser Irradiation Effect on the Structural and Optical Properties of Mg and MgO Nanoparticles Prepared Via Green Synthesis

Sahar Naji Rashid
Department of Physics, College of Science, University of Tikrit, Tikrit, Iraq

Received: 12/2/2024 Accepted: 19/1/2025 Published: 30/1/2026

Abstract

Laser processing of materials is currently one of the most interesting topics, especially with regard to nanomaterials. In this work, magnesium and magnesium oxide nanoparticles were irradiated with laser after they were synthesized using the green method to compare their characterization without and with laser exposure using some structural and optical characterization techniques. These nanoparticles were synthesized from magnesium chloride salt and saffron plant extract and then irradiated with a diode laser with three exposure periods (30, 60, and 90 sec). The results of the analyses showed that laser irradiation caused a reduction in the average grain sizes and diameters of the synthesized nanoparticles and the regularity of the surface morphology, in addition to an increase in their absorption, and this behavior increases with increasing the period of laser irradiation.

Keywords: Green synthesis, Laser irradiation, MgNPs, MgONPs, SPR.

تقييم تأثير التشعيع بالليزر على الخواص التركيبية والبصرية لجسيمات المغنيسيوم واوكسيد المغنيسيوم النانوية المحضرة بالطريقة الخضراء

سحر ناجي رشيد
قسم الفيزياء, كلية العلوم, جامعة تكريت, تكريت, العراق

الخلاصة

تعد معالجة المواد بالليزر في الوقت الحالي واحدة من أكثر المواضيع إثارة للاهتمام، خاصة فيما يتعلق بالمواد النانوية. في هذا العمل تم تشعيع جسيمات المغنسيوم وأوكسيد المغنسيوم النانوية بالليزر بعد تحضيرها بالطريقة الخضراء لمقارنة خصائصها قبل وبعد تعريضها لليزر باستخدام بعض تقنيات التوصيف التركيبي والبصري. تم تحضير هذه الجسيمات النانوية من ملح كلوريد المغنيسيوم ومستخلص نبات الزعفران ثم تم تشعيعها باستخدام ليزر الدايود بثلاث فترات تشعيع (30, 60, 90 sec). اظهرت النتائج ان التشعيع بالليزر أدى إلى انخفاض متوسط أحجام وأقطار الجسيمات النانوية المحضرة وانتظام تشكلها السطحي، بالإضافة إلى زيادة امتصاصيتها، وأن هذا السلوك يزداد مع زيادة فترة التشعيع بالليزر.

1. Introduction

Laser irradiation is one of the important material treatment applications, for which there are many research studies and continue to be developed [1]. The mechanism of laser

*Email: sahar83@tu.edu.iq

interaction with the irradiated material begins when the material absorbs most of the laser energy, then the electromagnetic energy is converted into electronic excitation, which turns into thermal, mechanical, and chemical energies [2,3]. In addition, the parameters of the laser can be controlled to influence the reaction environment, as well as the microstructure and shapes of the materials. Laser processing led to obtaining interesting morphologies and size modifications of nanoparticles (NPs) [4]. NPs are dispersion solutions of solid particles or atomic aggregates and have specific properties, like a high surface-to-mass ratio. Furthermore, their small size allows them to spread more freely in media [5]. In general, laser processing of nanoparticles in liquids is categorized into two types: the laser fragmentation of particles, which is produced by the laser energy absorbed by the involved particles themselves, as in Figure (1-a), and laser melting of particles, which increases the crystal size and reshapes them; this process can be utilized to melt nanoparticles or nanorods (NRs) into nanochains, as in Figure (1-b) [4].

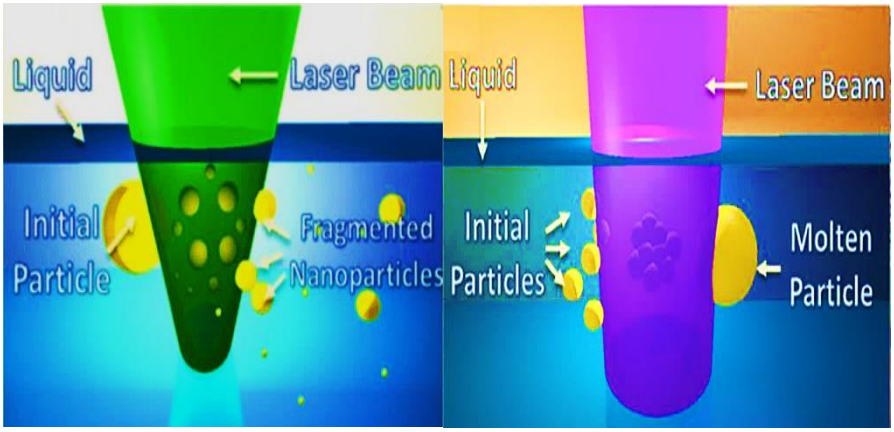

(a) **(b)**

Figure :1 laser processing of NPs in liquids (a) Fragmentation (b) Melting [4]

Most of the NPs studies are concerned with metal and metal oxide nanoparticles due to their unique properties, where they are used in many applications. Magnesium (Mg) and magnesium oxide (MgO) nanoparticles have recently attracted attention. In addition to the many advantages of magnesium, it has good dimensional stability and good properties at high temperatures [6,7]. Magnesium oxide nanoparticles (MgONPs) are important materials used in different applications, such as toxic waste remediation, catalysis, superconducting products, paint, and anti-bacterial activities. They can be prepared by chemical, physical, or biological synthesis [8-14]. Biological green synthesis of NPs has many advantages, such as being pollution-free, non-toxic, economical, environmentally friendly, and sustainable [15-17]. In addition to its use in foods, it has uses in various fields, including biological and medical, as well as in nanofabrication [18].

In this work, a diode laser beam was used to irradiate NPs prepared from aqueous magnesium chloride using biological green synthesis to investigate some physical characteristics without and after laser irradiation.

2. Materials and Methods

2.1 Biosynthesis of CS-(Mg & MgO)NPs

Aqueous magnesium chloride ($MgCl_2$) solution was prepared at a concentration of (1 M) by dissolving (0.4066 gm) of $MgCl_2$ in (20 ml) of deionized water on a hot plate magnetic stirrer device. Purified saffron (*Crocus sativus* L. (CS)) plant extract was prepared by adding (0.1 gm) of it in (10 ml) of deionized water and heating it for (5 min). The resulting extract

was filtered using a Whatman No.1 filter paper. After that, to obtain the nanoparticles, the extract solution was added to the $MgCl_2$ solution that was prepared with vigorous stirring for (15 min) at a temperature of approximately (50 °C), using a hot plate magnetic stirrer device, until the solution changes its color. The methods and procedures for the biosynthesis of metals and metal oxides nanoparticles can be summarized: the plant extract is mixed with the metal salt solution in conditions depending on the experiment, the metal particles are then reduced, and after that, the filtration step is carried out to obtain the metal at the nanoscale [15].

2.2 Laser Exposure

Four samples were prepared from the resulting nanoparticles solution, three of which were irradiated with a diode laser of a wavelength (808 nm) and a power of (1 W) at three different irradiation times (30, 60, and 90 sec). The distance between the laser source and the sample was (15 cm). The fourth sample was left without irradiation. Magnesium and its oxide show good absorbance in the near-infrared region [19,20], and the light intensity obtained from this wavelength of the diode laser is high [21].These two steps of the preparation method can be represented in a simplified diagram as in Figure (2).

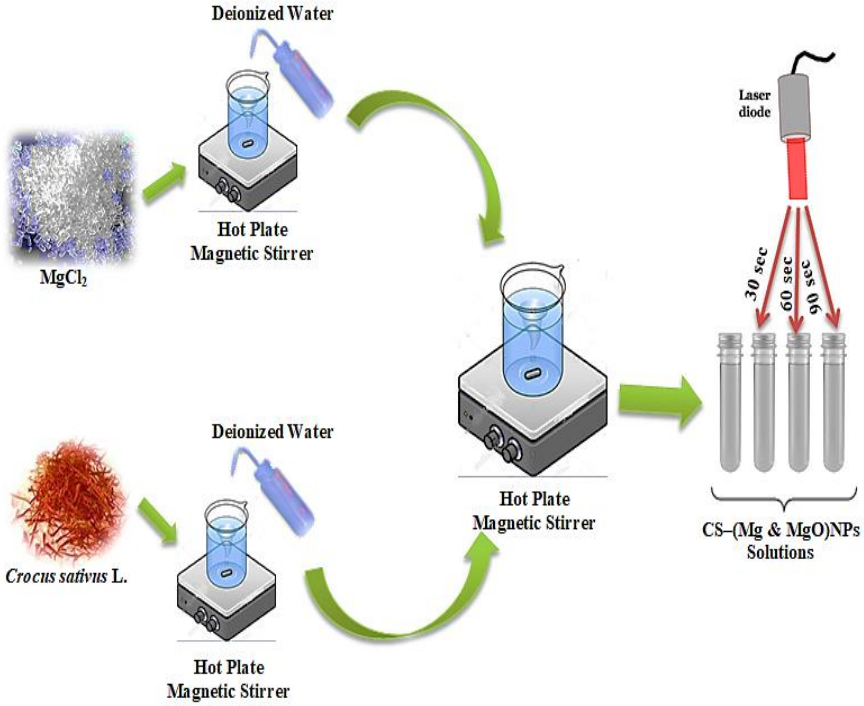

Figure 2: Simple schematic of MgNPs & MgONPs preparation

2.3 NPs Characterization

Structural and optical analyses were carried out for the four prepared samples using field Emission Scanning Electron Microscope (FESEM), Energy-Dispersive X-ray spectroscopy (EDX), X-ray Diffraction (XRD), Fourier-Transform Infrared Spectroscopy (FTIR), and UV-visible spectroscopy techniques.

3. Results and Discussion

3.1 XRD Analysis

The results of X-ray diffraction of the prepared NPs for the four samples showed that they have a polycrystalline structure, as in Figure (3). It is clear from this figure and through the appearance of diffraction peaks in the XRD patterns that the crystalline structure tends to be uniform when irradiated with laser, and the degree of this regularity increases with increasing

laser irradiation time [22]. Increasing the duration of laser irradiation improved the degree of material crystallization. In all apparent diffraction patterns, the formed diffraction angles and peaks indicate that they belong to magnesium hexagonal crystal structure according to JCPDS Card No. (00-035-0821), which is shaped as in Figure (4-a) [23], and magnesium oxide of cubic crystal structure according to JCPDS Card No. (01-078-0430), which is shaped as in Figure (4-b) [24]. In addition to the appearance of diffraction peaks in the three samples belonging to magnesium hydroxide of hexagonal crystal structure according to JCPDS Card No. (07-0239), which is shaped as in Figure (4-c) [25]. This agrees with the results of Abrinaei et al. [6], where, according to experimental works, the vapor is adsorbed chemically on the MgO surface, leading to the presence of vacancies in Mg. In this process, one molecule of water reacts with one molecule of MgO to form $Mg(OH)_2$. The intensity of the peaks represents the position of the atoms in the crystal structure. A change in phases leads to a change in the crystal structure and, thus, the disappearance of some peaks. Atoms in the crystal act individually as a light source similar to slits in a grating, so when the laser irradiation causes a decrease in the domain size, these atoms cause spots of different densities to appear; this may explain the difference in the number of peaks appearing in the diffraction patterns of the samples in Figure (3).

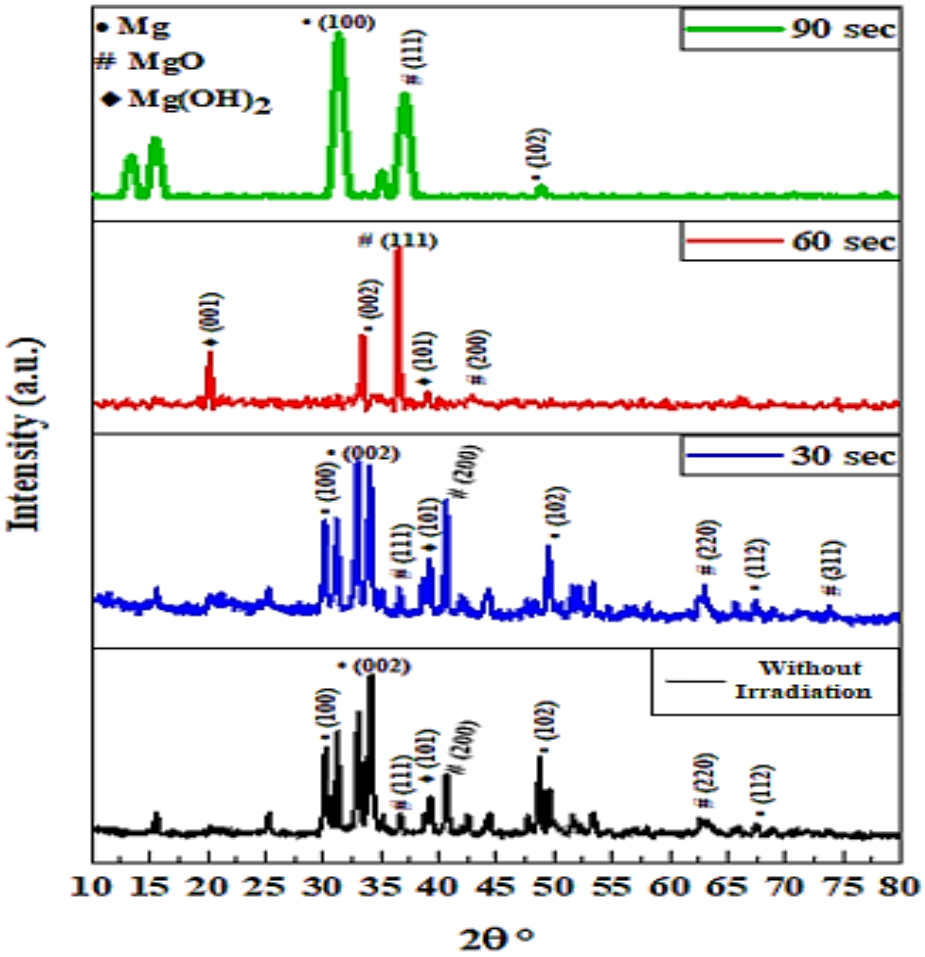

Figure 3 :XRD pattern of prepared NPs without and after laser irradiation at periods of 30, 60, and 90 sec

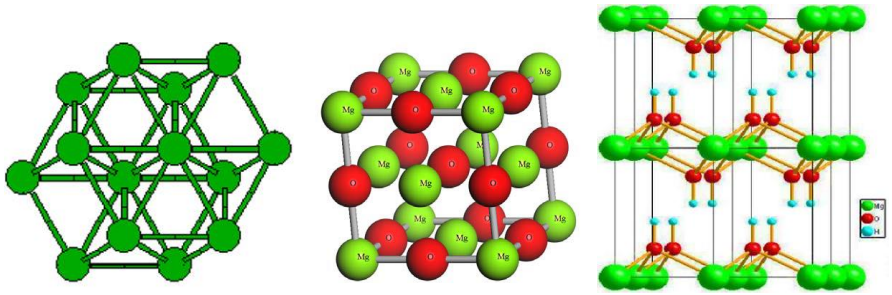

(a) **(b)** **(c)**

Figure 4 : Crystal structure (a) MgNPs, (b) MgONPs, (c) $Mg(OH)_2$NPs

Table (1) shows that the crystalline sizes of the prepared NPs decreased with increasing the laser irradiation period, as it was (27.8 nm) with no laser irradiation. It gradually decreased with increasing the period of laser irradiation, where it became (24.8 nm), (23.5 nm), and (7.4 nm) at irradiation periods of (30, 60, and 90 sec), respectively, agreeing with the results of Li et al. [4]. The crystalline size (D) was calculated using Scherer's equation as follows [8]:

$$D = \frac{0.9\lambda}{\beta cos\theta} \quad (1)$$

where λ is the X-ray wavelength (0.154 nm), θ is the Bragg diffraction angle, and β is the Full Width at Half Maximum (FWHM).

Table 1: Results of XRD pattern analysis of the manufactured NPs without and after irradiation at periods: 30, 60, and 90 sec

Laser Exposure Periods (sec)	*NPs*	*2θ (deg)*	*hkl*	*FWHM (deg)*	*d_{hkl} (nm)*	*D (nm)*
----	Mg	31	100	0.2952	0.286659	27.9
----	Mg	34	002	0.246	0.262356	33.8
----	MgO	36	111	0.246	0.244612	33.9
----	$Mg(OH)_2$	39	101	0.1968	0.229259	42.8
----	MgO	41	200	0.2952	0.212628	28.7
----	Mg	49	102	0.2952	0.183661	29.6
----	MgO	62	220	0.984	0.147959	9.4
----	Mg	68	112	0.6	0.138734	16
30	Mg	31	100	0.246	2.86428	33.5
30	Mg	34	002	0.4428	2.63095	18.8
30	MgO	36	111	0.3936	2.45172	21.2
30	$Mg(OH)_2$	39	101	0.1968	2.29748	42.8
30	MgO	41	200	0.246	2.22131	34.5
30	Mg	49	102	0.3444	1.83947	25.3
30	MgO	62	220	0.7872	1.47957	11.8
30	Mg	68	112	0.3936	1.38854	24.3
30	MgO	73	311	0.88	0.1294	11.2
60	$Mg(OH)_2$	22	001	0.25	3.79462	32.4
60	Mg	34	002	0.44	2.63095	18.9
60	MgO	36	111	0.394	2.45172	21.1
60	$Mg(OH)_2$	39	101	0.4	2.29748	21.1
60	MgO	41	200	0.35	2.22131	24.2
90	Mg	31	100	1.25	0.2881	6.6
90	MgO	36	111	1.25	0.2492	6.7
90	Mg	49	102	0.98	0.1857	8.9

3.2 FESEM Analysis

Figures (5, 6, 7, and 8) represent FESEM images (of different magnifications) of the prepared NPs with no laser exposure and at different laser exposure times of (30, 60, and 90 sec) of irradiation, respectively. It can be noted from Figure (6) that the green synthesized NPs were agglomerated in nature, as was also found by Wanga et al. [25], rod-like in shape, which agrees with Satheeshkumar et al. [26], with diameters averaging (58 nm). After irradiating these prepared NPs with a diode laser for different exposure times, little changes in their morphology were noticed, which agrees with Bdewi et al. [10]. The laser irradiation caused particle fragmentation, which resulted in the decrease in the NPs diameter averages as in Figures (6, 7, and 8) where they became (28, 22, and 12 nm) at irradiation periods of (30, 60, and 90 sec), respectively. Comparing the average sizes obtained from the results of FESEM with those of the XRD analysis, it was noticed that the results are generally similar in terms of decreasing. Although the rates obtained from the FESEM analysis results were larger as they represent the rates of the nanoparticle diameters, those obtained from the XRD analysis results represent the rates of the crystal sizes. FESEM measures the particle size on the surface, while XRD measures the crystal size inside the sample, since X-ray penetrates inside the sample; in addition to the fact that the particles are larger than the crystals.

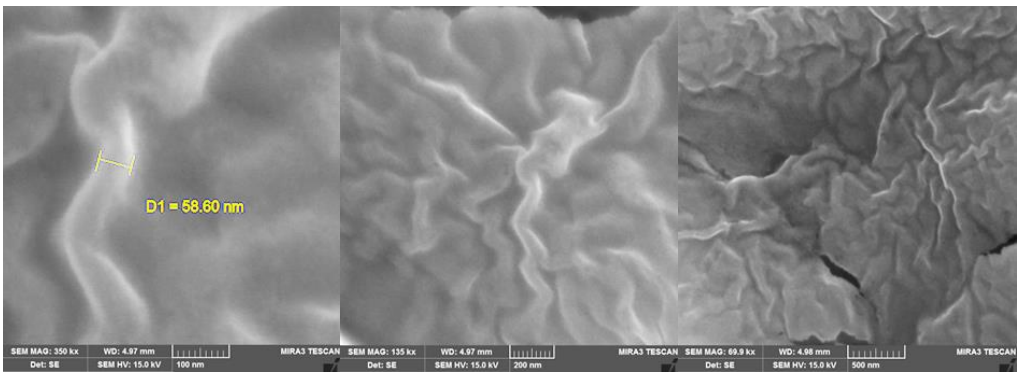

(a) **(b)** **(c)**

Figure5: FESEEM images of prepared NPs without laser irradiation with different magnifications (a) 100 nm, (b) 200 nm, (c) 500 nm

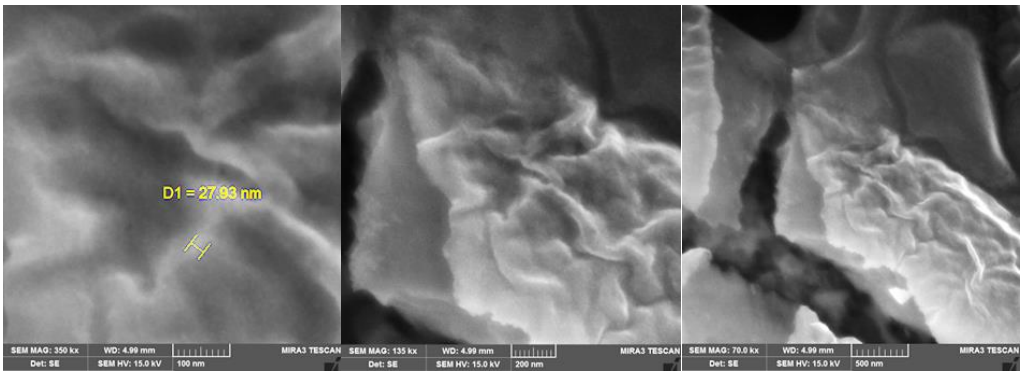

(a) **(b)** **(c)**

Figure 6: FESEEM images of prepared NPs at (30 sec) laser irradiation with different magnifications (a) 100 nm, (b) 200 nm, (c) 500 nm

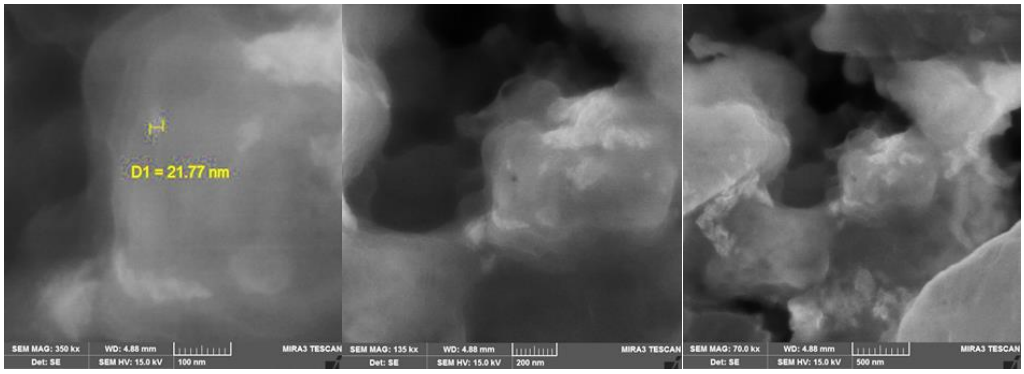

(a) (b) (c)

Figure 7: FESEEM images of prepared NPs at (60 sec) laser irradiation with different magnifications (a) 100 nm, (b) 200 nm, (c) 500 nm

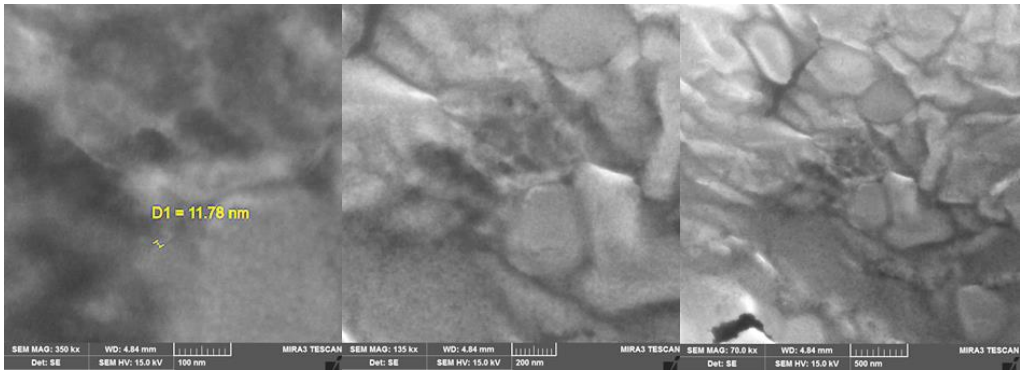

(a) (b) (c)

Figure 8: FESEEM images of prepared NPs at (90 sec) laser irradiation with different magnifications (a) 100 nm, (b) 200 nm, (c) 500 nm

3.3 EDX Analysis

Figure (9) represents EDX images of the NPs without and after laser irradiation. The analysis showed signals corresponding to Mg and O elements. The results indicated that the average percentages of O increased with the increase in the irradiation period. This result was also reached by Li et al. [4].

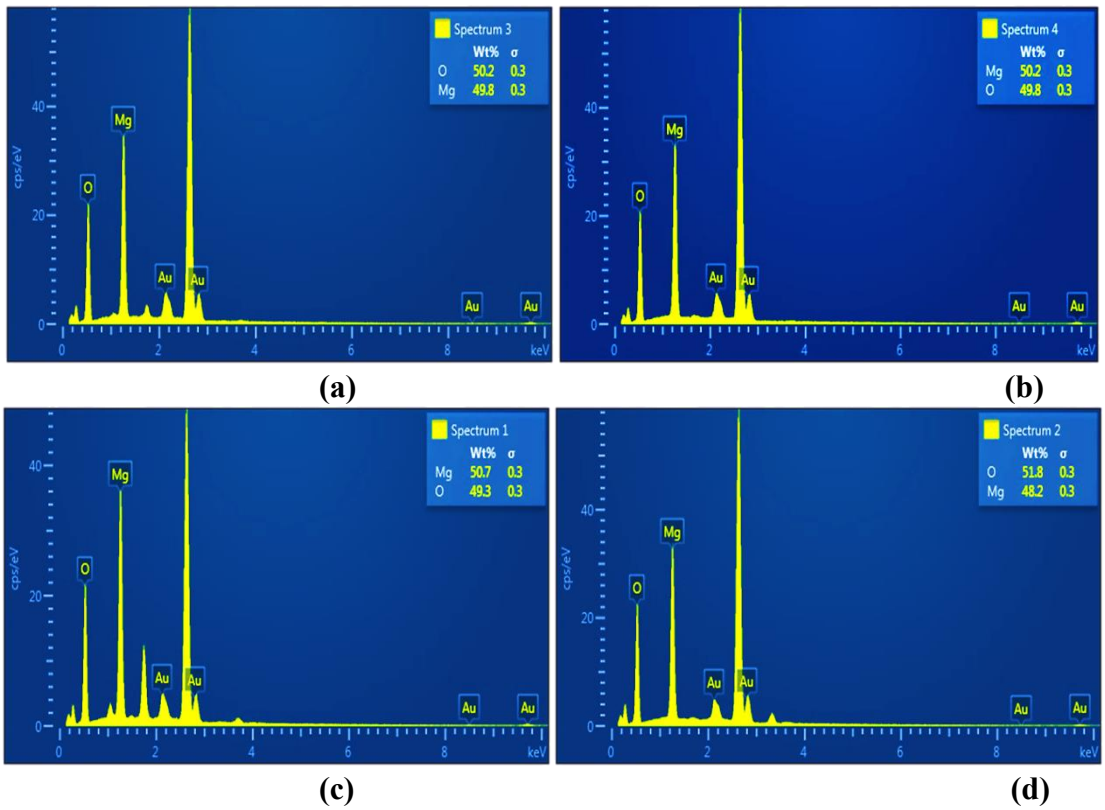

Figure 9: EDX images of the prepared NPs (a) without laser irradiation, (b) at (30 sec) of laser irradiation, (c) at (60 sec) of laser irradiation, (d) at (90 sec) of laser irradiation

3.4 FTIR Analysis

FTIR in the (400 – 4400 cm^{-1}) wavelength range was used to investigate MgNPs and MgONPs, as shown in Figure (10), which represents two spectra of the prepared NPs without and after (90 sec) of laser irradiation. At approximately (3460, 3420, 1630, 1150, 576, 520, 455, and 425 cm^{-1}), different absorption bands for the prepared NPs were detected, as was also done by Satheeshkumar et al. [26]. At high wavenumbers, the stretching vibration of the (O–H) bonds appeared; also, CO_2 stretching vibration appeared as a result of ambient carbon dioxide adsorption, and the existence of an (O–H) stretching mode of water was shown. The peak of magnesium hydroxide (Mg–OH) was noted at less than (1000 cm^{-1}). The detected peaks, which appeared from (576 to 425 cm^{-1}), confirmed the creation of (Mg–O) stretching vibrations. This result agrees with that of Wanga et al. [25] and Alterary et al. [27].

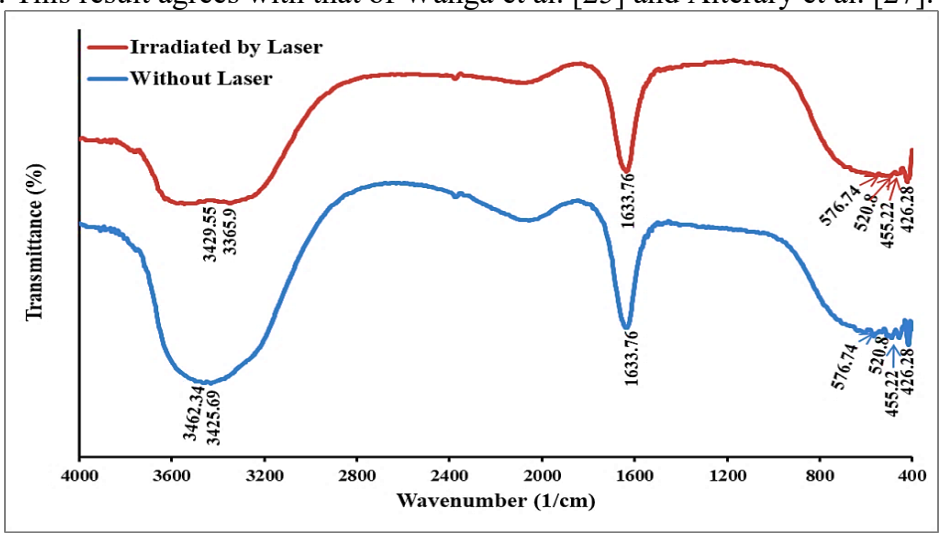

Figure 10 :FTIR spectra of the prepared NPs without and after (90 sec) of laser irradiation

3.5 UV-Vis Spectroscopy

Some optical properties of NPs without and after laser irradiation were analyzed using UV-Vis spectroscopy. The absorption spectra of the prepared NPs are shown in Figure (11). The peak representing the surface plasmon resonance (SPR) is highlighted; this peak represents the tuning of the frequencies of the nanoparticles' surface electrons with the frequencies of the illuminated light [28]. The position of the SPR in these spectra was between (322 – 330 nm) starting for the samples without laser irradiation (high value) and ending with those irradiated for the longest period of time. It is clear that SPR peak shifted towards short wavelengths and increased in width with increasing the irradiation period, which was the cause for the decrease in the diameter rates of NPs.

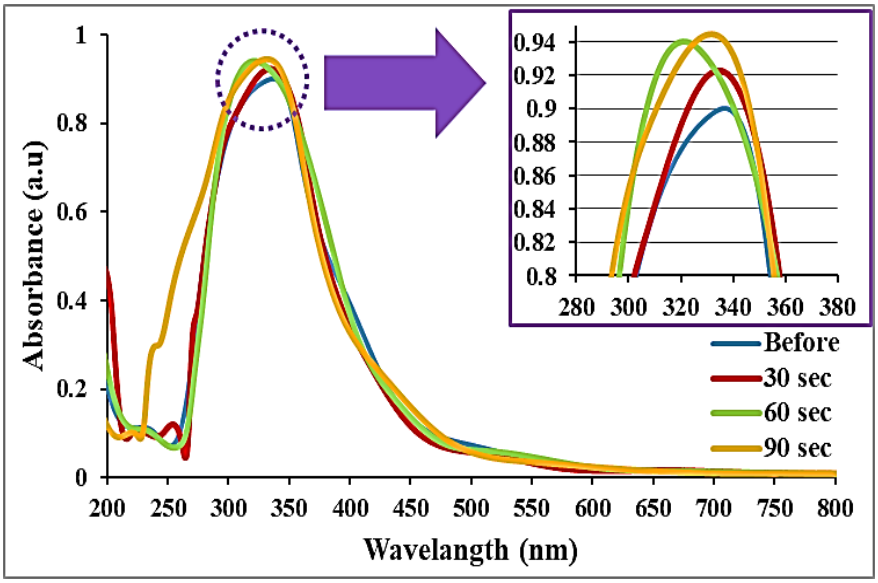

Figure 11: Absorbance spectra of the prepared NPs without and after laser irradiation

Transmittance spectra show behavior opposite to absorbance spectra, as shown in Figure (12). On the contrary, the absorption coefficient (α) curves, shown in Figure (13), are similar to the absorbance curves, as was also documented by Ali et al. [29]. The absorption coefficient was calculated from the following equation [29]:

$$\alpha = 2.303 \frac{A}{t} \quad (2)$$

where A = the absorption and t = the thickness or the light path through the sample. It is also clear from these curves that increasing the laser irradiation time, which in turn caused an increase in the laser flux, led to the rise in the value of the absorption coefficient of the prepared NPs.

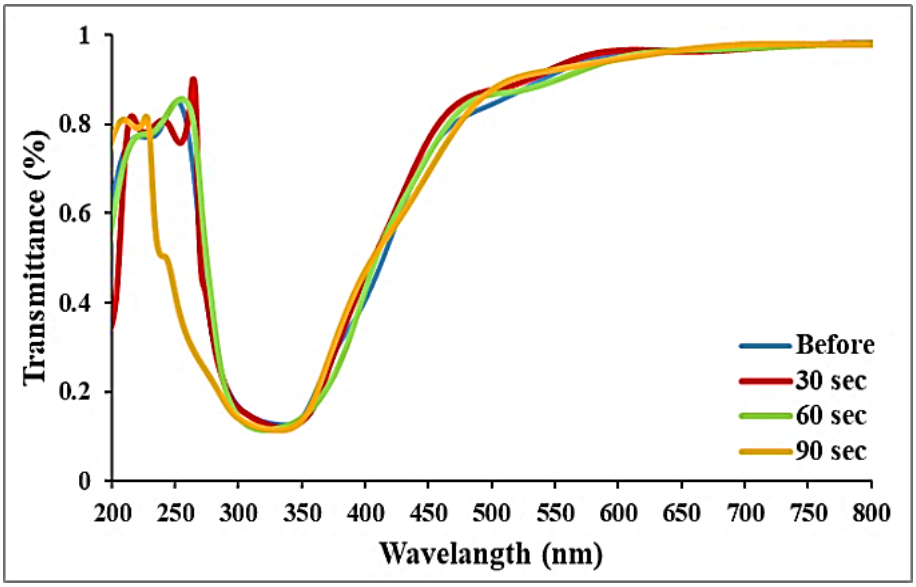

Figure 12: Transmittance spectra of the prepared NPs without and after laser irradiation.

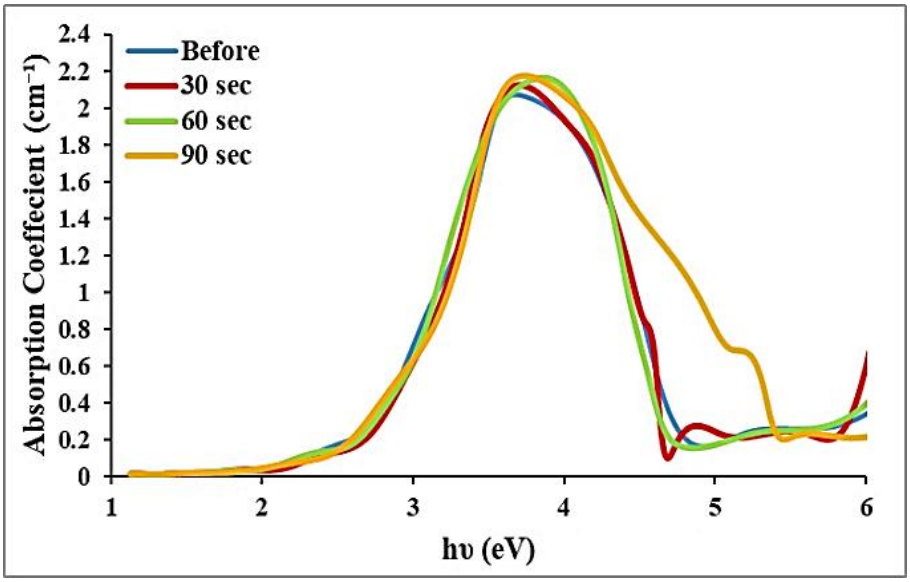

Figure 13: Absorption Coefficients of the prepared NPs without and after laser irradiation.

XRD results showed the peaks at diffraction angles belonging to MgONPs, from which their energy gap was calculated. Figure (14) represents the product of the absorption coefficient multiplied by the photon energy as a function of the photon energy. From the intersection of the tangent of the curve with the photon energy axis, the energy gap (Eg) of the prepared NPs was calculated without and after laser irradiation. It is clear that Eg rose with the irradiation time and also increased with the increase in laser flux. The increase in the energy gap values, which correspond to the increase in absorbance, resulted from the decrease in the size of the nanoparticles, which occurred as a result of the increase in the laser irradiation time. The increase in the energy gap values may mean recrystallization due to the increase in the laser flux.

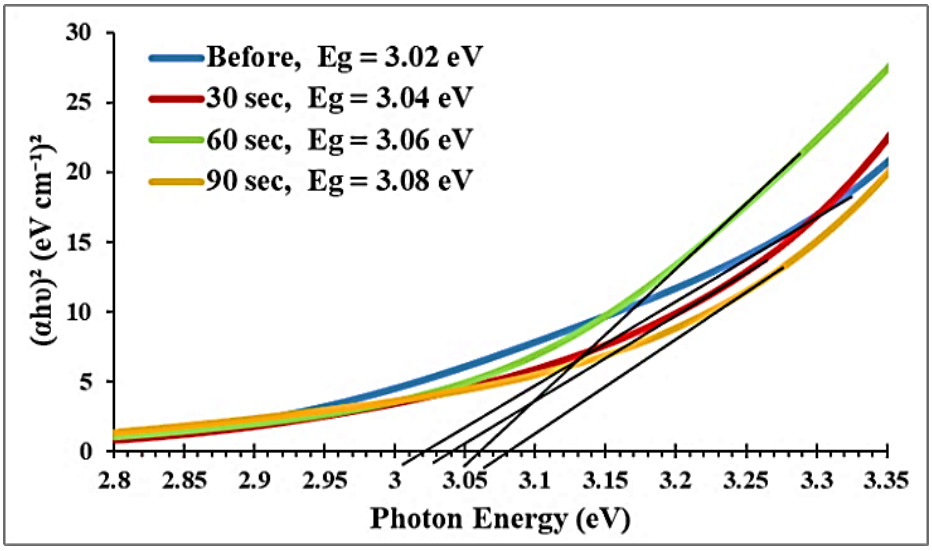

Figure 14: Energy gaps of the prepared NPs without and after laser irradiation

4. Conclusions

Enhancing the structural and optical properties of nanoparticles using laser beams is a good and promising result for controlling the advantages of nanoparticles and employing them for different applications by controlling the parameters of the laser used. A diode laser with a wavelength of (808 nm) and a power of (1 W) was used to irradiate the NPs with different irradiation times. It was found that it has an effect (albeit with slight changes sometimes) in characterizing magnesium and magnesium oxide nanoparticles prepared using the green method. It affects the averages of nanoparticle sizes, diameters, and absorbance, which can be used in various medical as an antimicrobials and anticancer cells, and in various industrial applications as a detector or gas sensor.

References

[1] M. Hasan, M. M. Hanafiah, Z. A. Taha, I. H. H. AlHilfy and M. N. M. Said, "Laser Irradiation Effects at Different Wavelengths on Phenology and Yield Components of Pretreated Maize Seed," *Applied Science* , vol. 10, no. 1189, pp. 1-12, 2020. https://doi.org/10.3390/app10031189.

[2] A. V. Kimel, Laser-Matter Interaction, Faculteit der Natuurwetenschappen Wiskunde en Informatica Opleiding: *Physics and Astronomy, Netherland*, 2020, p. 17.

[3] S. Krishnan and M. Mudrich, "Intense laser matter interaction in atoms, finite systems and condensed media: recent experiments and theoretical advances," *Eur. Phys. J. Spec. Top*., vol. 230, pp. 3981-3988, 2021. https://doi.org/10.1140/epjs/s11734-021-00364-x.

[4] L. Li, J. Zhang, Y. Wang, F. U. Zaman, Y. Zhang, L. Hou and C. Yuan, "Laser irradiation construction of nanomaterials toward electrochemical energy storage and conversion: Ongoing progresses and challenges," *WILEY*, vol. 3, pp. 393-1421, 2021. https://doi.org/10.1002/inf2.12218.

[5] S. Campora and G. Ghersi, "Recent developments and applications of smart nanoparticles in biomedicine," *Nanotechnology Reviews, DE Gruyter*, vol. 11, pp. 2595-2631, 2022. https://doi.org/10.1515/ntrev-2022-0148.

[6] F. Abrinaei, M. J. Torkamany, M. R. Hantezadeh and J. Sabbaghzadeh, "Formation of Mg and MgO Nanocrystals by Laser Ablation in Liquid: Effects of Laser Sources," *Science of Advanced Materials*, vol.4, pp. 501-506, 2012. https://doi.org/10.1166/sam.2012.1309.

[7] E. M. Sulaiman, F. Mutlak and U. Nayef, "High-performance photodetector of Au-MgO/PS nanostructure manufactured via Pulsed laser ablation Technique," *Optical and Quantum Electronics*, vol. 54, 744 (12 pages), 2022. https://doi.org/10.1007/s11082-022-04156-y.

[8] A. Almontasser, A. Parveen and A. Azam, "Synthesis, Characterization and antibacterial activity of Magnesium Oxide (MgO) nanoparticles," *IOP Conference Series: Materials Science and*

Engineering, vol. 577, 012051 (10 pages), 2019. https://doi.org/10.1088/1757-899X/577/1/012051.

[9] S. Yousefi, B. Ghasemi and M. P. Nikolova, "Opto-structural characterization of $Mg(OH)_2$ and MgO nanostructures synthesized through a template-free sonochemical method," *Applied Physics A*, vol. 549, 127 (10 pages), 2021. https://doi.org/10.1007/s00339-021-04605-7.

[10] S. F. Bdewi, O. G. Abdullah, B. K. Aziz and A. A. R. Mutar, "Synthesis, Structural and Optical Characterization of MgO Nanocrystalline Embedded in PVA Matrix," *Journal of Inorganic and Organometallic Polymers and Materials*, vol. 26, pp. 326-334, 2016. https://doi.org/10.1007/s10904-015-0321-3.

[11] K. Ganapathi, CH. Ashok, K. Venkateswara and CH. Shilpa, "Structural properties of MgO Nanoparticles: Synthesized by Co-Precipitation Technique," *International Journal of Science and Research (IJSR)*, vol. 4, no. 438, pp. 43-46, 2014. https://www.ijsr.net/conf/ATOM2014/ATOM2014_11.pdf.

[12] M. Amina, N. Musayeib, N. A. Alarfaj, M. F. El-Tohamy, H. F. Oraby, G. A. Al Hamoud, S. I. Bukhari and N. M. S. Moubayed, "Biogenic green synthesis of MgO nanoparticles using *Saussurea costus* biomasses for a comprehensive detection of their antimicrobial, cytotoxicity against MCF-7 breast cancer cells and photocatalysis potentials," *PLOS ONE*, vol. 15, no. 8, e0237567 (23 pages), 2020. https://doi.org/10.1371/journal.pone.0237567.

[13] R. Ali, Z. J. Shanan, G. M. Saleh and Q. Abass, "Green Synthesis and the Study of Some Physical Properties of MgO Nanoparticles and Their Antibacterial Activity," *Iraqi Journal of Science*, vol. 61, no. 2, pp. 266-276, 2020. https://doi.org/10.24996/ijs.2020.61.2.9.

[14] H. M. Abdulwahab, B. G. Rasheed and H. H. Altawil, "Deposition of MgO Nanoparticles by Laser Pyrolysis," *Al-Nahrain Journal for Engineering Sciences NJES*, vol. 25, no. 1, pp. 20-27, 2022. http://doi.org/10.29194/NJES.25010020.

[15] S. Ying, Z. Guan, P. C. Ofoegbu, P. Clubb, C. Rico, F. He and J. Hong, "Green synthesis of nanoparticles: Current developments and limitations," *Environmental Technology & Innovation*, vol. 26, 102336 (20 pages), 2022. https://doi.org/10.1016/j.eti.2022.102336.

[16] H. Chopra, S. Bibi, I. Singh, M. M. Hasan, M. S. Khan, Q. Yousafi, A. A. Baig, M. M. Rahman, F. Islam, T. Emran and S. Cavalu, "Green Metallic Nanoparticles: Biosynthesis to Applications," *Front. Bioeng. Biotechnol.*, vol. 10, 874742 (20 pages), 2022. https://doi.org/10.3389/fbioe.2022.874742.

[17] Y. M. Jebur and F. G. Abd, "Biosynthesis of MgO Nanoparticles by using Streptococcus Species and Its Antibacterial Activity," *Biochem. Cell. Arch.*, vol. 21, pp. 2557-2563, 2021. https://connectjournals.com/03896.2021.21.2557.

[18] R. Srivastava, H. Ahmed, R. Dixit, Dharamveer and S. A. Saraf, "*Crocus sativus* L.: A comprehensive review," *Pharmacognosy Reviews*, vol. 4, no. 8, pp. 200-208, 2010. https://doi.org/10.4103/0973-7847.70919.

[19] A. M. Hofmeister, E. Keppel and A. K. Speck, "Absorption and reflection infrared spectra of MgO and other diatomic compounds," *Mon. Not. R. Astron. Soc*., vol. 345, pp. 16-38, 2003. https://doi.org/10.1046/j.1365-8711.2003.06899.x.

[20] A. Khalid, R. Norello, A. N. Abraham, J. P. Tetienne, T. J. Karle, E. W. C. Lui, K. Xia, P. A. Tran, A. J. O'Connor, B. G. Mann, R. Boer, Y. He, A. M. Ching, A. B. Djurisic, R. Shukla and S. T. Hanic, "Biocompatible and Biodegradable Magnesium Oxide Nanoparticles with In Vitro Photostable Near-Infrared Emission: Short-Term Fluorescent Markers," *Nanomaterials*, vol. 9, no. 10, 1360 (16 pages), 2019. https://doi.org/10.3390/nano9101360.

[21] Z. Ren, Q. Li, B. Li and K. Song, "High wall-plug efficiency 808-nm laser diodes with a power up to 30.1 W," *Journal of Semiconductors*, vol. 41, no. 3, 032901 (5 pages), 2020, https://doi.org/10.1088/1674-4926/41/3/032901.

[22] K. I. Mohammed, A. S. Jasim and S. N. Rashid, "Effect of Annealing by CO_2 Laser on Structural and Optical Properties of CuO Thin Films Prepared by Sol – Gel Method," *International Journal of Physics*, vol. 4, no. 3, pp. 59-63, 2016. https://doi.org/10.12691/ijp-4-3-3.

[23] I. P. Jain, C. Lal and A. Jain, "Hydrogen storage in Mg: A most promising material," *International journal of hydrogen energy*, vol. 35, pp. 5133-5144, 2010. https://doi.org/10.1016/j.ijhydene.2009.08.088.

[24] H. Wei, L. Tang, M. Xiao and Y. Xu, "Fabrication and Characterization of Nano MgO Crystal," *Advances in Engineering Research*, vol. 122, pp. 12-17, 2017. https://doi.org/10.2991/icaset-17.2017.2.

[25] Q. Wanga, C. Lib, M. Guoa, S. Luoc and C. Hu, "Transesterification of dimethyl carbonate with phenol to diphenyl carbonate over hexagonal $Mg(OH)_2$ nanoflakes," *Inorganic Chemistry Frontiers*, vol. 1, pp. 1-29, 2015. https://pubs.rsc.org/en/content/articlelanding/2015/qi/c4qi00113c.

[26] D. Satheeshkumar, S. Velmurugan, K. Sathiyamoorthi and B. Dhinakaran, "Sustainable approach to Synthesis of Magnesium Nanoparticles (MgNPs) By Waste Peel Extracts of *Citrullus Lanatus* (Watermelon) and Photo-catalytic activity with Alizarin red dye," *Journal of Emerging Technologies and Innovative Research (JETIR)*, vol. 9, no. 5, pp. 443-449, 2022. https://www.jetir.org/view?paper=JETIR2205057.

[27] S. S. Alterary, M. F. El-Tohamy, G. A. E. Mostafa and H. Alrabiah, "Atropine-Phosphotungestate Polymeric-Based Metal Oxide Nanoparticles for Potentiometric Detection in Pharmaceutical Dosage Forms," *Nanomaterials*, vol. 12, 2313 (18 pages), 2022. https://doi.org/10.3390/nano12132313.

[28] A. Al-Sharqi, K. Apun, M. Vincent, D. Kanakaraju and L. Maurice Bilung, "Enhancement of the Antibacterial Efficiency of Silver Nanoparticles against Gram-Positive and Gram-Negative Bacteria Using Blue Laser Light," *International Journal of Photoenergy*, vol. 2019, 2528490 (12 pages), 2019. https://doi.org/10.1155/2019/2528490.

[29] R. S. Ali, H. S. Rasheed, N. D. Abdulameer, N. F. Habubi and S. S. Chiad, "Physical properties of Mg doped ZnS thin films via spray pyrolysis," *Chalcogenide Letters*, vol. 20, no. 3, pp. 187-196, 2023. https://doi.org/10.15251/CL.2023.203.187.